Electronic supplementary information (EIS)

Metal-Organic Frameworks for the capture of α-pinene traces

Patrick P. Conti,[a,b] Kamal Batra,[a] Paul Iacomi,[a] Carla Vieira Soares,[a] Sanchari Dasgupta,[c] Nathalie Steunou,[c] Agnès Lattuati-Derieux,[d] Noëlle Timbart,[d] Mélanie Nicolas,[b], Rukshala Anton,[b] Stéphane Moularat,[b] Guillaume Maurin,[a] and Sabine Devautour-Vinot [a,*]

a. Institut Charles Gerhardt Montpellier (ICGM), UMR 5253 – CNRS/UM/ENSCM, Pole Chimie Balard Recherche, 34293 Montpellier cedex 5, France
b. Centre Scientifique et Technique du Bâtiment (CSTB), 24 rue Joseph Fournier, 38400 Saint-Martin-d'Hères, France
c. Institut Lavoisier de Versailles (ILV), Université de Versailles ST Quentin en Yvelines, Université Paris Saclay, 78035 Versailles cedex, France
d. Centre de Recherche et de Restauration des Musées de France (C2RMF), Département Recherche, Palais du Louvre, 14 quai François Mitterrand, 75001 Paris, France

Contents

1 MATERIALS

1.1 Reagents, solvents and analyte

2-Aminoterephthalic acid and benzene1,4-dicarboxylic acid (terephthalic acid) were purchased from Thermo Fisher Scientific.Titanium isopropoxide and zirconium propoxide were purchased from Sigma Aldrich. N,N'-Dimethylformamide, methanol and absolute ethanol were purchqsed from Carlo Erba Reagents, France. All reagents and solvents were used as received from the commercial suppliers without further purification.
α-pinene, 98% purity, was purchased from Sigma-Aldrich.

1.2 MOFs

DUT-4
DUT-4 was purchased from Materials Center (TU Dresden, Germany).

Synthesis of MIL-125(Ti)-NH_2

MIL-125(Ti)-NH_2 nanoparticles (NPs) were synthesized according to the previously reported protocol.[1]
1.41 g of 2-aminoterephthalic acid was dispersed in 20 mL of DMF and 5 mL of methanol in a 100 mL round-bottom flask. The organic linker was stirred until its complete dissolution. Then 1.5 mL of titanium isopropoxide was added to the linker solution followed by 0.1 mL of distilled water. The reaction mixture was heated at 100 °C for 96 hours. The as-synthesized MOF NPs were washed with DMF and absolute ethanol. The MIL-125-NH_2(Ti) NPs were dispersed in absolute ethanol.

Synthesis of UiO-66(Zr)
UiO-66(Zr) NPs were synthesized according to the previously reported method.[2]
In a 20 mL scintillation vial, 71 µL of 70% zirconium propoxide solution in 1-propanol, 7 mL of DMF and 4 mL of acetic acid were added. The solution was heated at 130 °C for 2 h. A noticeable color change was observed from colorless to yellow. The solution was cooled to room temperature. To this solution, 75 mg of benzene1,4-dicarboxylic acid linker was added and was dispersed by ultrasound for 30 sec and allowed to stir for 18 h at 25 °C. The MOF was then recovered by centrifugation and was washed several times with DMF and ethanol. The NPs were stored in ethanolic suspension.

2 METHODS

2.1 MOF characterizations

Powder X-Ray Diffraction Patterns were collected on a Siemens D5000 X'Pert MDP diffractometer r (λ_{Cu}, $K_{\alpha1}$, $K_{\alpha2}$) for a range of 2θ from 5 to 40°. Powder X-Ray Diffraction (PXRD) patterns were also collected on a Panalytical X'Pert PRO PXRD diffractometer, with a Cu radiation source in a Bragg-Brentano reflection geometry, employing a spinning sample holder with a low-background silicon insert. Infrared spectra were recorded on a FTIR Magna 550 Nicolet spectrophotometer with diamond tip at a resolution of 4 cm^{-1}. Nitrogen porosimetry data were collected on a Micromeritics Tristar at 77 K (The MOFs were activated at 423 K under vacuum for 5 hours). The thermal stability of the samples were analyzed on a thermogravimetric analyzer, Model Perkin Elmer SDA 6000 by heating the sample upto 700 °C with a heating rate of 3 °C min^{-1} under oxygen atmosphere.

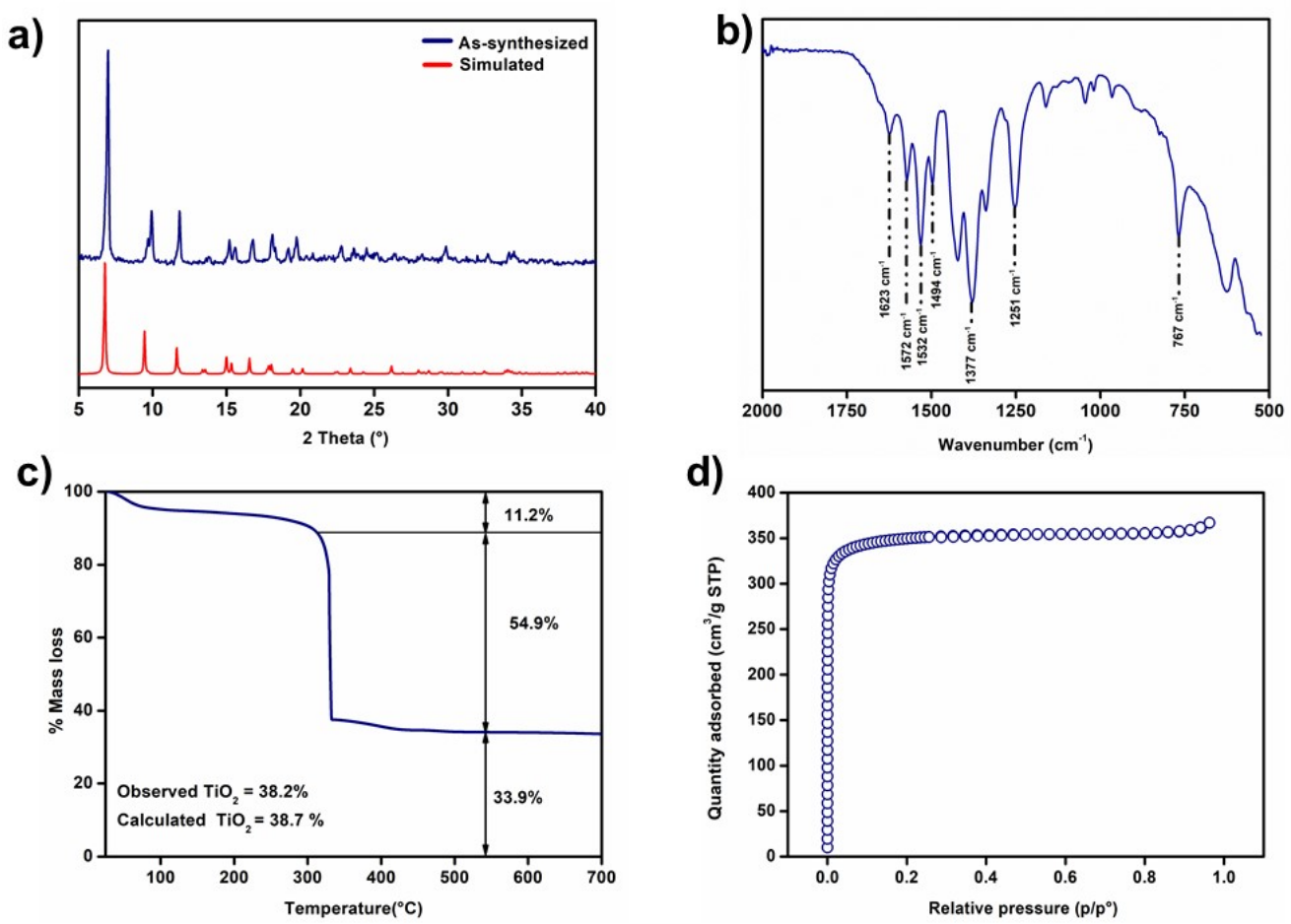

Figure S1. a) PXRD pattern, **b)** FT-IR spectrum, **c)** Thermogravimetric analysis, and **d)** Nitrogen porosimetry of MIL-125(Ti)-NH_2 NPs.

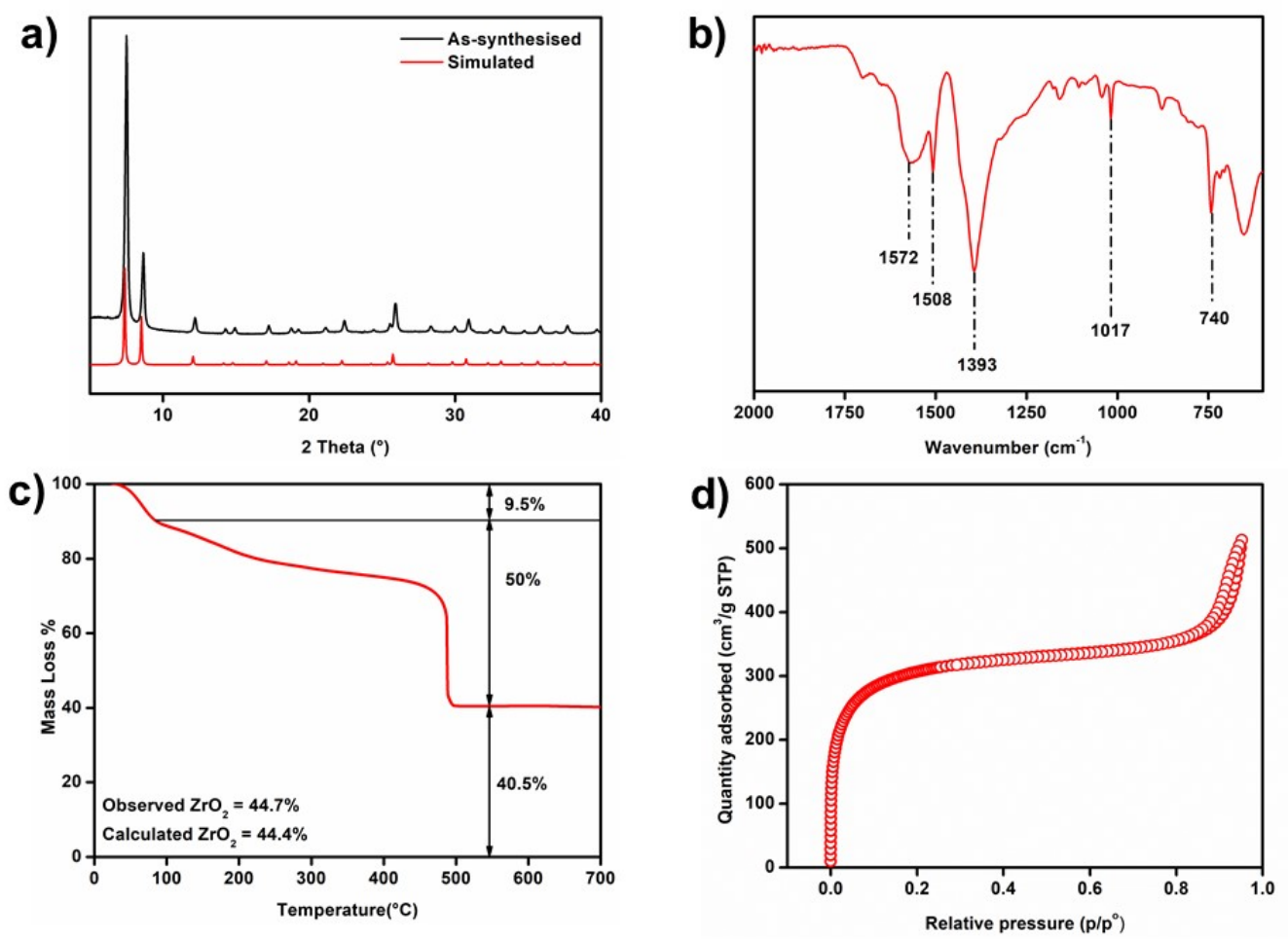

Figure S2. a) PXRD pattern, **b)** FT-IR spectrum, **c)** Thermogravimetric analysis, and **d)** Nitrogen porosimetry of UiO-66(Zr) NPs.

2.2 Pinene sorption

Pinene adsorption isotherms were carried out at 303 K using a DVS vacuum apparatus from Surface Measurement Systems. In this equipment, an argon flow passes through a temperature-controlled reservoir containing liquid α-pinene. A continuous α-pinene/argon flow driven by a vacuum system, enters the sample chamber and passes through the suspended sample pan. The pressure is controlled by a butterfly valve located before the outlet. Noteworthy, a calibration procedure was applied to evaluate the degree of α-pinene saturation in the gas carrier (Part 4). The sample mass is monitored by a magnetically suspended balance with ±0.1 µg resolution. Approximately 20-30 mg of sample are introduced inside a stainless-steel sample pan, placed in the DVS chamber, and further *in situ* activated at 423 K for 2 hr under vacuum conditions (10^{-2} Pa).

As the α-pinene partial pressure in the bubbler headspace might be lower than its saturation pressure (P_{sat} = 803 Pa at 303K), a calibration procedure is required. Two sorption isotherms, considering pure vapour and the bubbler carrier mixture configurations, were collected on a reference material, i.e. PCN-777. Both isotherms are adjusted by a scaling factor until the two isotherms overlap in the α-pinene concentration region showing sharp increase of the analyte uptake ($C_{\alpha\text{-pinene}}$ > 500 ppm).

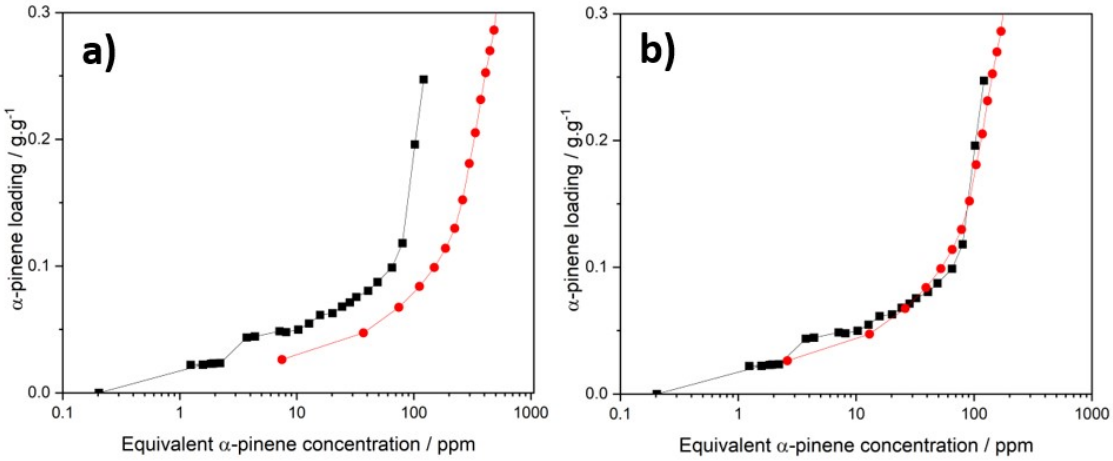

Figure S3: α-pinene adsorption isotherms for PCN-777 at 303 K, using the pure vapour (red circles) and the bubbler carrier mixture (black squares) configurations **a)** before and **b)** after adjustment.

2.3 DFT calculations

The crystal structures of UiO-66(Zr), MIL-125(Ti)NH_2, Cr-soc-mof, MIL-68(Al), DUT-4(Al), and DUT-5(Al) were taken from previous papers.[3–6] The full geometry optimizations (atomic positions and unit cell volumes) of all these MOFs were performed at the Density Functional Theory (DFT) level, as implemented in the Vienna *Ab initio* Simulation Package (VASP)[7–9] along with a plane-wave basis set and projector augmented wave (PAW) pseudopotentials.[10] The Perdew-Burke-Ernzerhof (PBE)[11] functional was employed while the electron wave functions were expanded using the plane waves with an energy cutoff of 450 eV. The DFT-D3 method of the Grimme van der Waals correction including Becke–Johnson damping (BJ) was used to account for the long-range interactions.[12,13] The convergence of total energy and the force between atoms were set to 10^{-5} eV and 0.01 eV $Å^{-1}$, respectively. The Γ-centered k-point mesh with a size of 1x1x1 grid was used to sample the Brillouin zone during DFT optimization. The same methodology was applied to identify the preferential adsorption site of 1 pinene molecule loaded in the simulation box of all MOFs made of 1x1x1 unit cells. Several starting configurations for α-Pinene were considered in the different cages and pore positions to ensure that we converge towards the most energetically stable configuration for each MOF-loaded system.

The DFT interaction energy (E_{int}) between α-Pinene and the different MOFs was calculated by means of the following equation :

$$\mathbf{E_{int} = E_{MOF/\,\alpha\text{-}Pinene} - (E_{MOF} + E_{\alpha\text{-}Pinene})}$$

where, $E_{MOF/\alpha\text{-}Pinene}$ is the total energy of the MOF/ α-Pinene adduct, E_{MOF} and $E_{\alpha\text{-}Pinene}$ are the corresponding energies of the single components.

2.4 Monte Carlo simulations

All Monte Carlo simulations were performed using the simulation code CADSS (Complex Adsorption and Diffusion Simulation Suite).[14] All atoms of the MOF frameworks were treated as a charged Lennard-Jones (LJ) interacting sites with LJ parameters taken from Universal Force Field (UFF)[15] and DREIDING[16] force field for the inorganic and the organic nodes respectively. The partial charges for the framework structures were extracted from periodic DFT calculations coupled with the density derived electrostatic and chemical (DDEC)[17,18] method as implemented in the CHARGEMOL module.[19–22] The LJ cross parameters corresponding to the interactions between the guest and the MOF framework were obtained using the Lorentz−Berthelot mixing rules. α-pinene was described by a united atom representation including LJ point charges with parameters taken from the OPLS-all atom force field.[23] The α-pinene affinity for all MOFs were assessed using the Widom insertion method[24] that enabled to assess the adsorption enthalpy at 25 ºC using $2x10^8$ production and equilibration cycles. Complementary MC simulations were carried out in the NVT ensemble to explore the preferential adsorption sites of α-pinene for MIL-125(Ti)-NH_2, UiO-66(Zr) and DUT-4(Al) at different loadings corresponding to the experimental values obtained at different concentration levels in the adsorption isotherms. For each state point, $2x10^8$ Monte Carlo steps were for both equilibration and production runs.

3 MOFs CHARACTERIZATION AFTER PINENE ADSORPTION

3.1 MIL-125(Ti)-NH_2

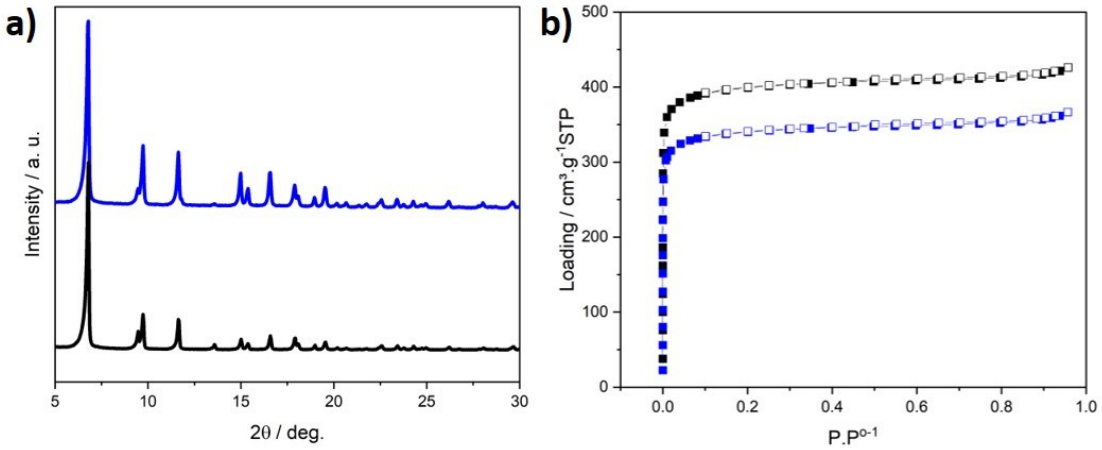

Figure S4: a) PXRD pattern for MIL-125(Ti)-NH_2 as-activated (black line) and after α-pinene sorption experiments (blue line). **b)** Nitrogen sorption isotherms recorded at 77K for MIL-125(Ti)-NH_2 as activated (black square) and after α-pinene sorption experiments (blue square). Filled and open squares refer to the adsorption and the desorption branches, respectively.

3.2 UiO-66(Zr)

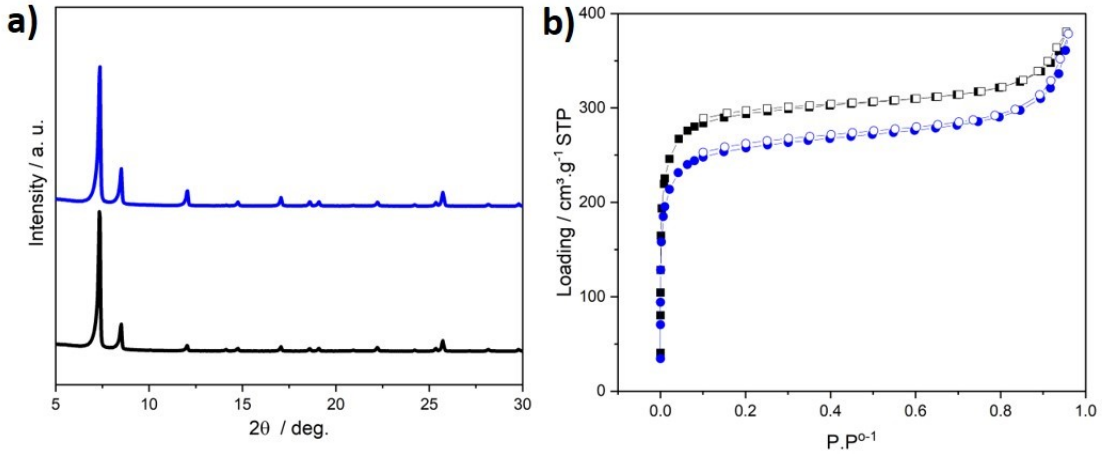

Figure S5: a) PXRD pattern for UiO-66(Zr) as-activated (black line) and after α-pinene sorption experiments (blue line). **b)** Nitrogen sorption isotherms recorded at 77K for UiO-66(Zr) as activated (black square) and after α-pinene sorption experiments (blue square). Filled and open squares refer to the adsorption and the desorption branches, respectively.

3.3 DUT-4(Al)

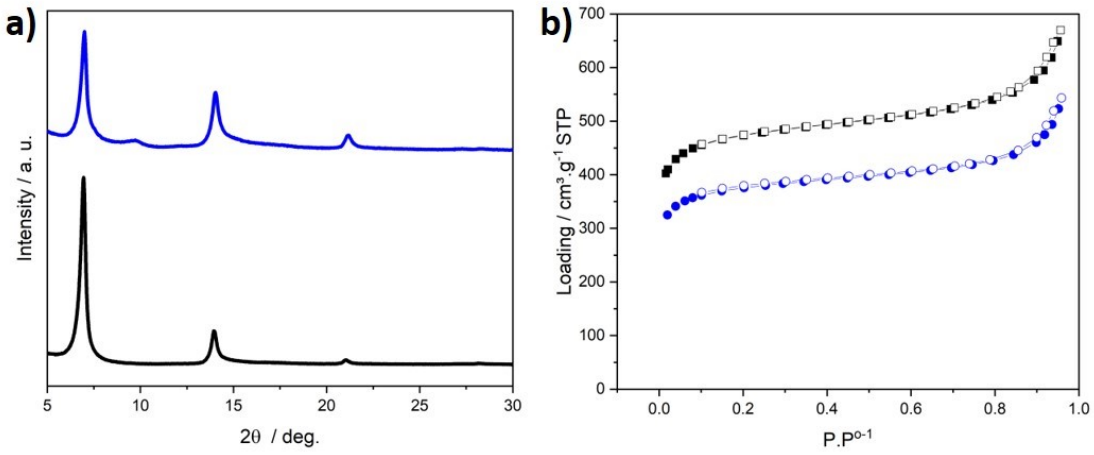

Figure S6: a) PXRD pattern for DUT-4(Al) as-activated (black line) and after α-pinene sorption experiments (blue line). **b)** Nitrogen sorption isotherms recorded at 77K for DUT-4(Al) as activated (black square) and after α-pinene sorption experiments (blue square). Filled and open squares refer to the adsorption and the desorption branches, respectively.

Table SI – Experimental textural properties of MIL-125(Ti)-NH_2, DUT-4(Al) and UiO-66(Zr) deduced from N_2 sorption experiments. Comparison with the theoretical N_2-accessible surface area and free pore volume obtained from the crystal structure applying a geometric approach according to the Zeo ++ software.[25]

MOF Structures	**S_{BET} / m^2g^{-1}**		**V_{pore} / cm^3g^{-1}**		**N_2 accessible surface / m^2g^{-1}**	**V_{pore} / cm^3g^{-1}**
	Pristine	**After α-pinene sorption**	**Pristine**	**After α-pinene sorption**	**Pristine**	
MIL-125(Ti)-NH_2	1574[a]	1319[a]	0.62	0.53	1728	0.65
UiO-66(Zr)	1150[a]	1004[a]	0.46	0.40	1102	0.38
DUT-4(Al)	1816[a]	1443[a]	0.73	0.58	2094	0.69

[a] Samples were activated at 423 K for 8 h

The small discrepancy in the S_{BET} and V_{pore} values for samples explored before and after α-pinene sorption is due to the possible presence of remaining α-pinene molecules within the pore structures.

4 MONTE CARLO CONFIGURATIONS FOR α-PINENE IN UiO-66(Zr) AND DUT-4(Al)

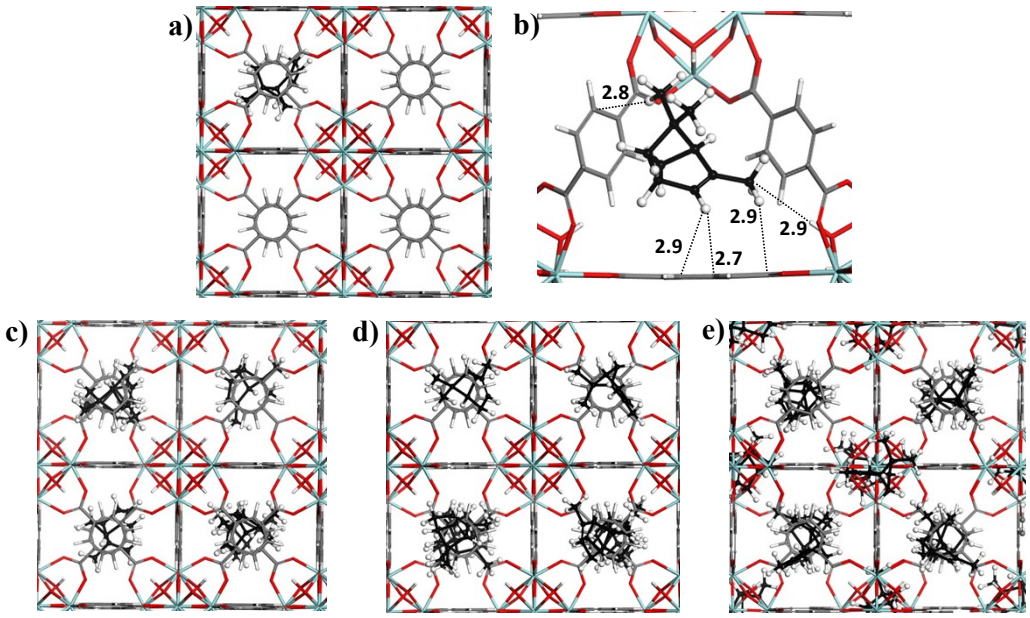

Figure S7: Monte Carlo configurations for α-pinene in UiO-66(Zr) at different analyte loadings determined from the experimental adsorption isotherm at **a)** low concentration (0.10 g/g = 0.75 mmol/g) and **b)** host-guest interacting distances reported in Å, **c)** 1.6 ppm (0.16 g/g = 1.17 mmol/g), **d)** 24 ppm (0.30 g/g = 2.23 mmol/g), and **e)** high concentration (0.43 g/g = 3.14 mmol/g).

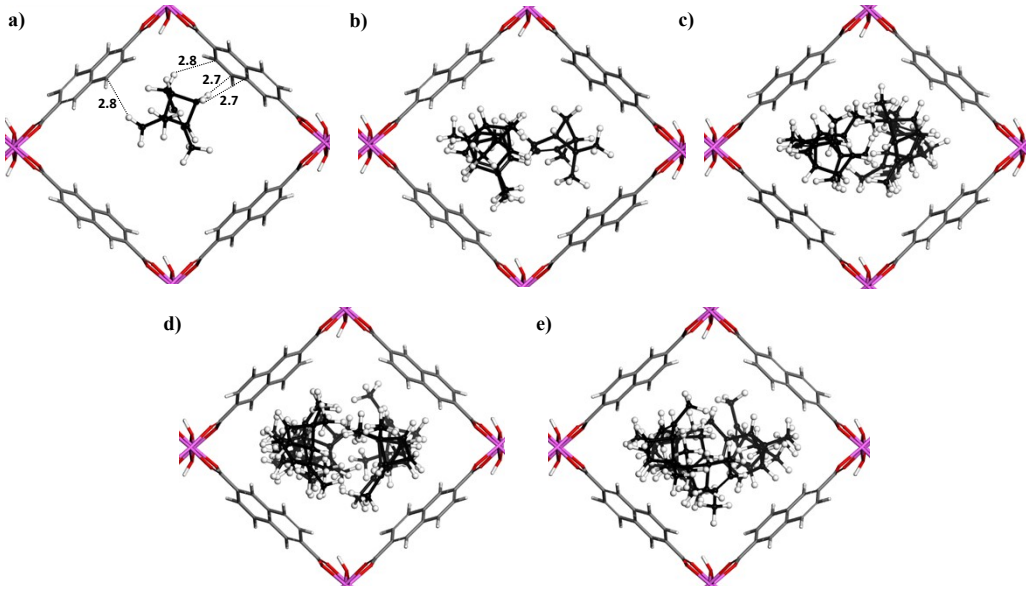

Figure S8: Monte Carlo configurations for α-pinene in DUT-4(Al) at different analyte loadings determined from the experimental adsorption isotherm at **a)** low concentration (0.018 g/g = 0.13 mmol/g), **b)** 0.8 ppm (0.026 g/g = 0.19 mmol/g), **c)** 1.6 ppm (0.11 g/g = 0.85 mmol/g), **d)** 24 ppm (0.31 g/g = 2.30 mmol/g), and **e)** 240 ppm (0.37 g/g = 2.71 mmol/g).

5 MIL-125(Ti)-NH_2 REGENERATION

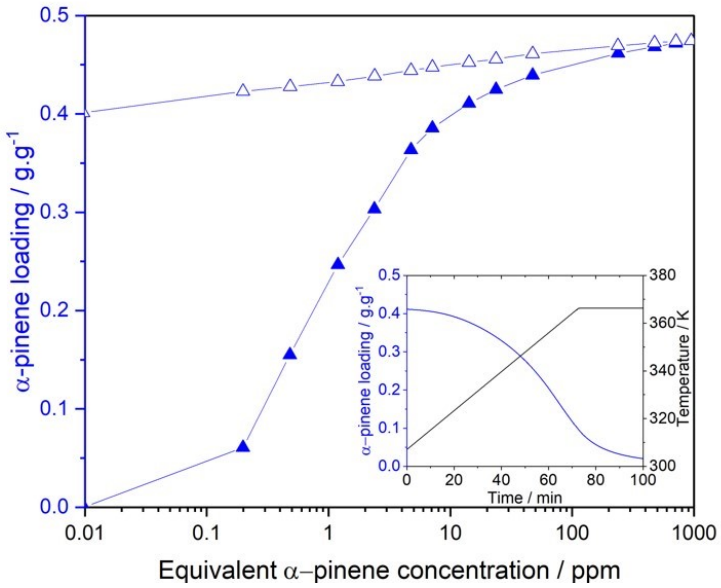

Figure S9 Gravimetric sorption isotherm of α-pinene collected at 303 K on MIL-125(Ti)-NH_2. Filled and empty triangles represent adsorption and desorption branches, respectively. The inset shows the mass loss due to α-pinene release, upon heating the solid from 303 K to 373 K, under secondary vacuum.

References:

1 S. M. F. Vilela, P. Salcedo-Abraira, I. Colinet, F. Salles, M. C. De Koning, M. J. A. Joosen, C. Serre and P. Horcajada, *Nanomaterials*, 2017, **7**, 321.

2 S. Biswas, M. Haouas, C. Freitas, C. Vieira Soares, A. Al Mohtar, A. Saad, H. Zhao, G. Mouchaham, C. Livage, F. Carn, N. Menguy, G. Maurin, M. L. Pinto and N. Steunou, *Chem. Mater.*, 2022, **34**, 9760–9774.

3 P. G. Yot, K. Yang, F. Ragon, V. Dmitriev, T. Devic, P. Horcajada, C. Serre and G. Maurin, *Dalt. Trans.*, 2016, **45**, 4283–4288.

4 D. Cunha, M. Ben Yahia, S. Hall, S. R. Miller, H. Chevreau, E. Elkaïm, G. Maurin, P. Horcajada and C. Serre, *Chem. Mater.*, 2013, **25**, 2767–2776.

5 Q. Yang, S. Vaesen, M. Vishnuvarthan, F. Ragon, C. Serre, A. Vimont, M. Daturi, G. De Weireld and G. Maurin, *J. Mater. Chem.*, 2012, **22**, 10210–10220.

6 J. Wieme, K. Lejaeghere, G. Kresse and V. Van Speybroeck, *Nat. Commun.*, 2018, **9**, 4899.

7 G. Kresse and J. Hafner, *Phys. Rev. B*, 1993, **47**, 558–561.

8 G. Kresse and J. Furthmüller, *Phys. Rev. B - Condens. Matter Mater. Phys.*, 1996, **54**, 11169–11186.

9 G. Kresse and J. Hafner, *Phys. Rev. B*, 1994, **49**, 14251–14269.

10 P. E. Blöchl, *Phys. Rev. B*, 1994, **50**, 17953–17979.

11 J. P. Perdew, A. Ruzsinszky, G. I. Csonka, O. A. Vydrov, G. E. Scuseria, L. A. Constantin, X. Zhou and K. Burke, *Phys. Rev. Lett.*, 2008, **100**, 136406.

12 A. D. Becke and E. R. Johnson, *J. Chem. Phys.*, 2005, **123**, 154101.

13 S. Grimme, S. Ehrlich and L. Goerigk, *J. Comput. Chem.*, 2011, **32**, 1456–1465.

14 Q. Yang, D. Liu, C. Zhong and J. R. Li, *Chem. Rev.*, 2013, 113.

15 A. K. Rappé, C. J. Casewit, K. S. Colwell, W. A. Goddard and W. M. Skiff, *J. Am. Chem. Soc.*, 1992, **114**, 10024–10035.

16 S. L. Mayo, B. D. Olafson and W. A. Goddard, *J. Phys. Chem.*, 1990, **94**, 8897–8909.

17 T. A. Manz and D. S. Sholl, *J. Chem. Theory Comput.*, 2012, **8**, 2844–2867.

18 T. A. Manz and D. S. Sholl, *J. Chem. Theory Comput.*, 2010, **6**, 2455–2468.

19 T. A. Manz and N. G. Limas, *RSC Adv.*, 2016, **6**, 47771–47801.

20 N. G. Limas and T. A. Manz, *RSC Adv.*, 2016, **6**, 45727–45747.

21 T. A. Manz, *RSC Adv.*, 2017, **7**, 45552–45581.

22 N. G. Limas and T. A. Manz, *RSC Adv.*, 2018, **8**, 2678–2707.

23 W. L. Jorgensen, D. S. Maxwell and J. Tirado-Rives, *J. Am. Chem. Soc.*, 1996, **118**, 11225–11236.

24 T. J. H. Vlugt, E. García-Pérez, D. Dubbeldam, S. Ban and S. Calero, *J. Chem. Theory Comput.*, 2008, **4**, 1107–1118.

25 T. F. Willems, C. H. Rycroft, M. Kazi, J. C. Meza and M. Haranczyk, *Microporous Mesoporous Mater.*, 2012, **149**, 134–141.